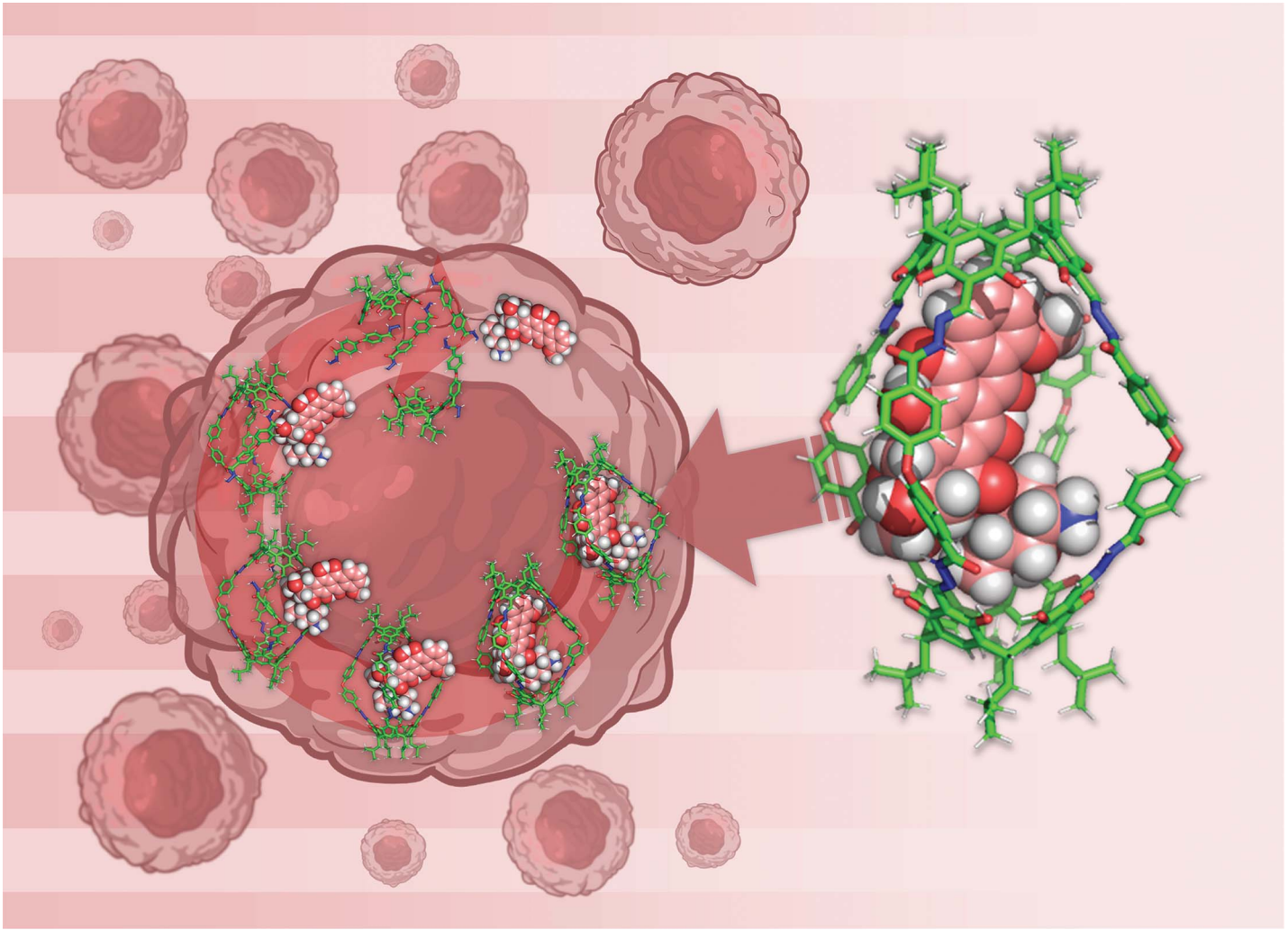

Showcasing research from Vicente Martí Centelles and Ramón Martínez Máñez, IDM- Universitat Politècnica de València and CIBER-BBN, Spain.

Comparing organic and metallo-organic hydrazone molecular cages as potential carriers for doxorubicin delivery

Our work describes a rare comparative study between a metallo-organic cage and a fully organic analogous system, both obtained by hydrazone bond formation self-assembly. The organic cage shows better properties, including stability and affinity towards the anticancer drug doxorubicin. Additionally, the organic cage shows minimal cell toxicity, whilst the doxorubicin-cage complex shows *in vitro* anti-cancer activity. Our results show that the properties of the organic cage are suitable for the future challenges of *in vivo* drug delivery using molecular cages. Cancer cell image created with BioRender.com.

As featured in:

See Ramón Martínez-Máñez, Vicente Martí-Centelles *et al.*, *Chem. Sci.*, 2024, **15**, 10010.

ROYAL SOCIETY OF CHEMISTRY

rsc.li/chemical-science

Registered charity number: 207890

Chemical Science

ROYAL SOCIETY OF CHEMISTRY

EDGE ARTICLE

View Article Online
View Journal | View Issue

Cite this: *Chem. Sci.*, 2024, **15**, 10010

All publication charges for this article have been paid for by the Royal Society of Chemistry

Comparing organic and metallo-organic hydrazone molecular cages as potential carriers for doxorubicin delivery†

Giovanni Montà-González, [aef] David Bastante-Rodríguez, [ac] Alba García-Fernández, [abc] Paul J. Lusby, [f] Ramón Martínez-Máñez [*abcde] and Vicente Martí-Centelles [*abe]

Molecular cages are three-dimensional supramolecular structures that completely wrap guest molecules by encapsulation. We describe a rare comparative study between a metallo-organic cage and a fully organic analogous system, obtained by hydrazone bond formation self-assembly. Both cages are able to encapsulate the anticancer drug doxorubicin, with the organic cage forming a 1 : 1 inclusion complex with μM affinity, whereas the metallo-organic host experiences disassembly by interaction with the drug. Stability experiments reveal that the ligands of the metallo-organic cage are displaced in buffer at neutral, acidic, and basic pH, while the organic cage only disassembles under acidic conditions. Notably, the organic cage also shows minimal cell toxicity, even at high doses, whilst the doxorubicin-cage complex shows *in vitro* anti-cancer activity. Collectively, these results show that the attributes of the pure organic molecular cage are suitable for the future challenges of *in vivo* drug delivery using molecular cages.

Received 5th April 2024
Accepted 6th June 2024

DOI: 10.1039/d4sc02294g

rsc.li/chemical-science

Introduction

Supramolecular chemistry has been largely driven by the design and study of host molecules that use non-covalent interactions for efficient guest binding.[1,2] For over 60 years, the structures of synthetic hosts have changed enormously, evolving from acyclic, macrocyclic, to fully three-dimensional cage structures that completely wrap guest molecules.[3,4] Despite the challenges of synthesis, the development of efficient self-assembly methods has enabled the synthesis of cages with almost any possible geometry.[5–7] Self-assembly allowed preparing molecular cages by the design of ligands with a specific shape to self-assemble into metallo-cages and purely organic cages.[5,6] For this, it is possible to use either reversible metal–ligand interactions, to give coordination cages, or dynamic covalent chemistry to yield purely organic cages.[8,9]

Cage synthesis is mainly based on the self-assembly of building blocks with complementary connectivity and geometry under thermodynamic control.[10] Many studies on molecular cages have focused on establishing efficient synthetic protocols, allowing multigram-scale production of cages in some cases, facilitating large-scale synthesis for different applications.[11,12] Moreover, the careful design of the building blocks allows a precise control of the cavity size, shape, and inward-facing functionalisation for selective and efficient encapsulation.[13–15] Main uses of molecular cages include catalysis,[16–19] stabilisation of species,[20,21] molecular recognition,[5,6] release of encapsulated guests,[5,6,22] sensing,[23] separation processes,[13,24,25] among many others.[26,27] However, the exploration of molecular cages in biological and biomedical contexts remains nascent.[5,6,28–32]

Preparing cages for bio-medical applications presents a unique set of challenges, most obviously developing systems that are compatible with biological conditions, such as the prerequisite for water solubility.[5,6,33] In general, fully organic cages have low solubility in water due to their lack of charge and hydrophobic nature, requiring water solubilizing groups in some instances or the use of organic cosolvents.[5] In contrast, metallo-cages are typically charged species that can result in

[a]*Instituto Interuniversitario de Investigación de Reconocimiento Molecular y Desarrollo Tecnológico (IDM), Universitat Politècnica de València, Universitat de València, Camino de Vera, s/n, 46022, Valencia, Spain. E-mail: vimarce1@upv.es*

[b]*CIBER de Bioingeniería Biomateriales y Nanomedicina (CIBER-BBN), Instituto de Salud Carlos III, 28029, Madrid, Spain*

[c]*Unidad Mixta UPV-CIPF de Investigación en Mecanismos de Enfermedades y Nanomedicina, Valencia, Universitat Politècnica de València, Centro de Investigación Príncipe Felipe, Avenida Eduardo Primo Yúfera, 3, 46012, Valencia, Spain*

[d]*Unidad Mixta de Investigación en Nanomedicina y Sensores, Universitat Politècnica de València, Instituto de Investigación Sanitaria La Fe (IISLAFE), Avenida Fernando Abril Martorell, 106, 46026, Valencia, Spain*

[e]*Departamento de Química, Universitat Politècnica de València, Camí de Vera s/n, 46022, Valencia, Spain. E-mail: rmaez@qim.upv.es*

[f]*EaStCHEM, School of Chemistry, Joseph Black Building, David Brewster Road, EH93FJ, Edinburgh, UK*

† Electronic supplementary information (ESI) available. CCDC 2295536. For ESI and crystallographic data in CIF or other electronic format see DOI: https://doi.org/10.1039/d4sc02294g

water solubility without water solubilizing groups or cosolvents.[6] Another challenge is the dilution effects and the presence of biological analytes that can also produce significant issues to the integrity of systems that are often inherently dynamic (despite cooperative chelate effects).[5,6,56]

Despite the challenges, the research developed in recent years shows the feasibility of using molecular cages for *in vitro* applications, with some examples of *in vivo* treatments.[28,29,34,35] The versatility of cage assemblies holds the promise to overcome common drawbacks of conventional anticancer drugs, such as poor solubility and stability in physiological environments,[36,37] overcome drug resistance,[38] and reduce side effects on healthy tissues.[39] Some relevant examples include metallo-organic cages for anticancer drug delivery (*e.g.*, cisplatin, oxaliplatin, 5-fluorouracil, (+)-camptothecin, $(acac)_2Pd$, $(acac)_2Pt$, caffeine, *etc.*),[40–48] metallo-organic cages for intracellular release of photosensitizers,[49,50] crystalline nanoparticles formed by organic cages for removing doxorubicin and irinotecan by complexation,[51] and Pd_2L_4 and Pt_2L_4 cages with native toxicity against cells.[52,53] Despite the work carried out in the field, research focuses on only one type of cage, particularly on metallo-organic cages, and the comparison between fully organic cages and metallo-organic cages remains unexplored.

Here we report a comparative study of a fully organic cage and a metallo-organic cage, focusing on their host–guest properties, cage stability, and cellular toxicity (Fig. 1). Both systems are based on four dihydrazine "struts", yet they differ in the C_4 symmetric building block that serve to cap these units; the metal–organic cage exploits a square planar tetrapyridyl Pd(II) motif whereas the organic cage uses a calixarene. In this work we have tested the water-solubility of the cages, the affinity to encapsulate the anticancer drug doxorubicin, the cellular toxicity of the unloaded cages and the therapeutic activity of the fully organic cage loaded with doxorubicin. To the best of our knowledge this is the first comparative report of similarly shaped organic and metallo-organic cages, focusing on doxorubicin encapsulation and cell toxicity.

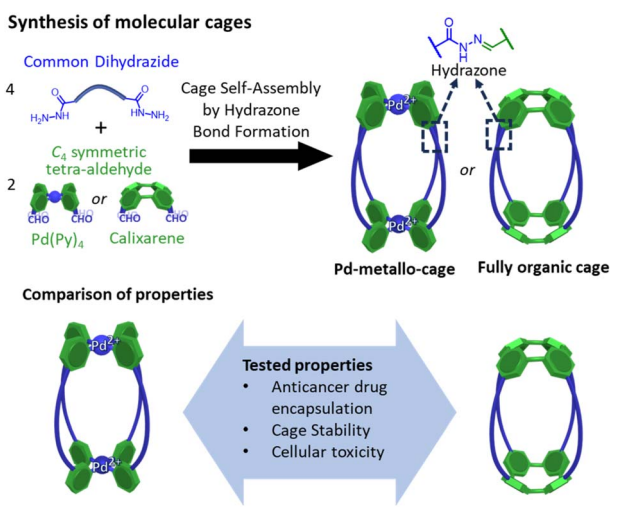

Fig. 1 Synthesis of molecular cages containing hydrazone bonds showing the main objective of the work focused on the comparison of properties of a metallo-cage with a fully organic cage.

Results and discussion

Synthesis of cages

In the design of the cages, we were interested in selecting a water-stable chemical group obtainable through a reversible reaction, to self-assemble the target structure from the corresponding building blocks. A structure containing hydrazone groups appeared an ideal choice, as these bonds are several order of magnitude more hydrolytically stable compared to groups such as imines at neutral pH,[54,55] yet are still dynamic under acidic conditions (pH 5 or below).[8,54,56–59] Cages containing hydrazone groups will remain stable in healthy tissues where the pH is in the range of 7.3–7.4, whereas cage breakdown will take place inside cells in the lysosomes (pH of *ca.* 4.5). The design might also be useful in targeting some human tumors with pH values as low as 5.6, although most frequent values are in the range of 6.4–7.[60]

Based on this idea, we designed two similarly shaped molecular cages (**C1** and **C2**) by the self-assembly of 4 dihydrazide ligands (**1**) with 2 tetra-aldehyde derivatives (**2** or **3**) (Fig. 2). Both cage forming reactions occur overnight at room temperature in DMSO. When ligand **1** is reacted with

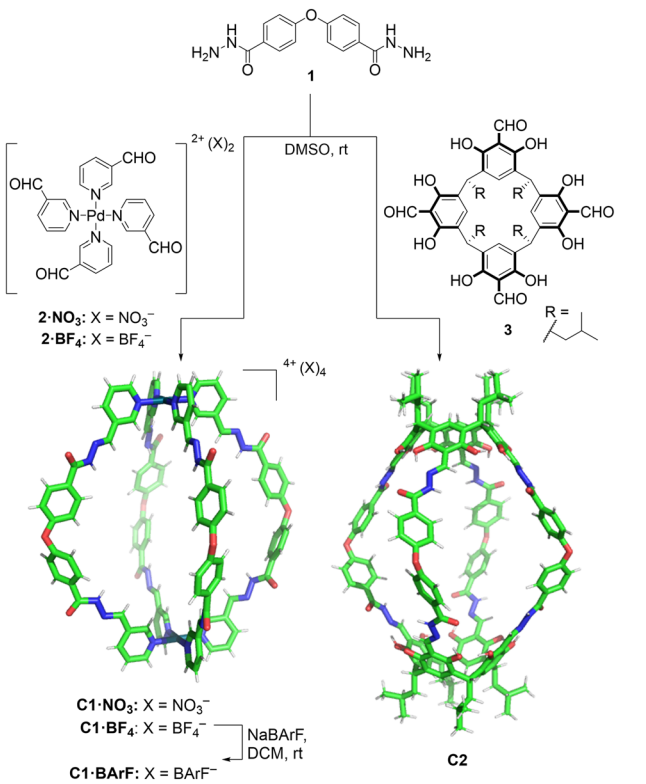

Fig. 2 Self-assembly of molecular cages **C1** and **C2** by hydrazone bond formation. The figure shows X-ray crystal structure of $C1{\cdot}NO_3$ cage (counteranions removed for clarity) while the **C2** cage structure was obtained from Spartan MMFF molecular modelling (see ESI† for X-ray and molecular modelling details).

nicotinaldehyde–Pd complex **2**, then Pd_2L_4 assembly **C1** is obtained. The solubility of **C1** can be controlled using different counteranions; the BArF cage **C1·BArF**, prepared *via* anion metathesis of **C1·BF_4**, is soluble in organic solvents,[16] whereas the nitrate cage **C1·NO_3**, obtained directly from the reaction of **1** and **2·NO_3**, can dissolve in aqueous mixtures containing DMSO. Organic cage **C2** was obtained by the reaction of **1** and calixarene starting material **3**. This cage is soluble in both organic solvents and in aqueous mixtures containing DMSO. For both cages it is required typically 1–5% DMSO in water to achieve μM concentration. All cages were fully characterised by ^{1}H, ^{13}C, DOSY NMR, and HRMS (see ESI†).

Additionally, the formation of the molecular cage **C1·NO_3** was unambiguously confirmed by X-ray crystallography (Fig. 2, see ESI† for details). The crystal structure of the **C1·NO_3** cage shows a quasi-spherical geometry, with a Pd–Pd distance of 18.6 Å and a *trans* ether O–O separation of 19.9 Å. In this structure, all the hydrazone NH bonds are pointing into the cavity of the cage, providing potential sites for polar interactions with an encapsulated guest. While we have been unable to grow XRD quality crystals of **C2**, a molecular model (X-ray structure shown in Fig. 2, additional details are available in the ESI†) indicates that the size and shape of the organic cage is similar to **C1**; the distance between the centroids of the two calixarene motifs is 18.8 Å while the *trans* ether O atoms are separated by 19.7 Å.

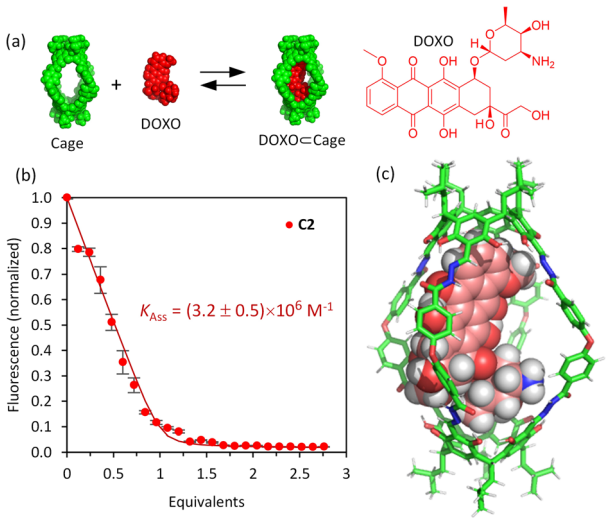

Fig. 3 Fluorescence titration experiments. (a) Schematic representation of drug encapsulation; (b) binding data for the encapsulation of DOXO by cage **C2** obtained from the fluorescence spectra for the addition of **C2** to DOXO (50 μM) in 100 μM phosphate buffer, pH 7.2. The solid points are experimental data, and the continuous lines is the fitted binding isotherm for a 1 : 1 host–guest model, obtained as the average of 4 independent titrations (vertical bars show the standard error for each point). Fluorescence measured at 590 nm with λ_{exc} = 470 nm (phosphate buffer 100 μM/DMSO 0.25–2.0%, pH 7.2); (c) MMFF molecular model of the supramolecular complex [DOXO⊂**C2**] obtained with the Spartan'20 software.

Host–guest chemistry

The affinity of the cages towards DOXO was assessed by means of titration experiments.[61] The photophysical properties of DOXO, which has a fluorescence emission maximum at 590 nm (λ_{exc} = 470 nm), enabled the use of emission change to quantify encapsulation of the guest, which was also confirmed by ^{1}H NMR studies. Both **C1·NO_3** and **C2** are soluble in the range 20–100 μM in phosphate buffer (buffer concentration 100 μM) with 1–5% v/v DMSO. As the absorption spectra of the molecular cages and DOXO do not overlap (Fig. S32 and S33†), quantitative fluorescence titrations of DOXO with increasing amounts of molecular cages were performed. The titrations with both **C1·NO_3** and **C2** show a DOXO fluorescence emission decrease (Fig. S28 and S29†). This is attributed to the presence of electron-poor Pd[(pyridine)$_4$]$^{2+}$ moieties in cage **C1·NO_3** and electron-rich resorcinol rings in cage **C2**, that quench the DOXO emission. The quenching can take place by intermolecular photo-induced electron transfer (PET) process as we estimated using the Rehm–Weller equation (see ESI†).[62,63]

The fluorescence quenching experiments reveal a significant difference between cages **C1·NO_3** and **C2**. The decrease in fluorescence emission was much more noticeable for **C2** compared to **C1·NO_3**, showing more efficient fluorescence quenching. Fitting the emission intensity *versus* the concentration of added cage to a 1 : 1 binding isotherm[64] using R and RStudio,[65,66] we determined an association constant of 3.2 × 10^6 M^{-1} for the organic cage **C2** (Fig. 3). For cage **C1·NO_3**, we estimated an association constant in the order of magnitude of 10^4 M^{-1} with low reproducibility, likely associated to cage disassembly by complexation of Pd^{2+} by the NH_2 moiety of DOXO as observed by NMR titrations (Fig. S24 and S28†). The increase of affinity is likely associated with the more hydrophobic nature of uncharged cage **C2** in contrast to the tetracationic **C1·NO_3**.[67] The inward facing NH groups of **C1·NO_3**, as determined from the X-ray crystal structure, could also lead to an energetically more favourable hydration of the cavity, leading to poorer DOXO binding. The high association constant of DOXO with **C2** permitted a Job's plot analysis to confirm the 1 : 1 stoichiometry of [DOXO⊂**C2**] (see ESI Fig. S30†), which is also supported by molecular modelling, suggesting that DOXO fits into the cavity of cage **C2** (Fig. 3c, see ESI† for molecular modelling details).

To check cavity occupancy by the guest, the cavity volume of both cages was determined using the CageCavityCalc Python script. The calculations gave 1350 Å^3 for cage **C1** and 1500 Å^3 for cage **C2**, showing that both cages have a similar cavity space.[68] As the size of DOXO is 498 Å^3, the single guest occupancy for **C1** and **C2** would be 37% and 33%, respectively, significantly less than the optimal 55% predicted by Rebek for closed-shell organic hosts.[69] Therefore, the binding observed does not follow the 55%-rule as cages **C1** and **C2** have very large portals, differing from the closed-shell hosts used to develop the 55%-rule.[15]

It is also possible to trigger the decomplexation of [DOXO⊂**C2**] by adding increasing amounts of DMSO (Fig. 4a). This causes the fluorescence intensity to increase, presumably because the exclusion of DOXO reduces quenching. From this data, we estimated that *ca.* 70% DOXO is released when the solution reaches 55% v/v DMSO (Fig. 4b). The decrease in

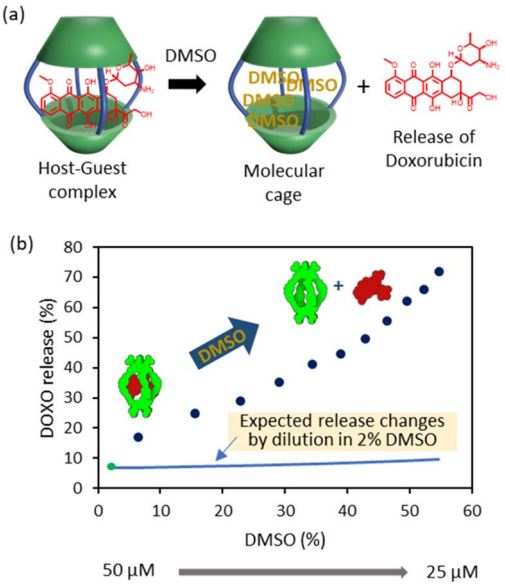

Fig. 4 DOXO release experiments. (a) Schematic representation of DOXO release by competition with DMSO molecules. (b) Plot of recovery of non-bound DOXO *versus* percentage of added DMSO (6–55%) to the solution containing **C2** ($C_{initial}$ = 50 μM, C_{final} = 25 μM) and DOXO ($C_{initial}$ = 50 μM, C_{final} = 25 μM) in phosphate buffer (1 mM, pH 7.2). The green dot indicates the release at 2% DMSO as determined in the binding experiments of Fig. 3. The blue line indicates the expected release changes by dilution from 50 μM to 25 μM in a solution containing 2% DMSO.

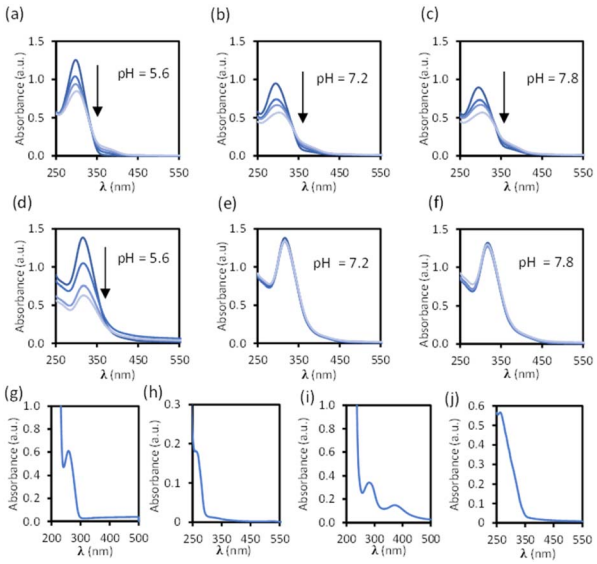

Fig. 5 Stability of cages **C1**·NO_3 (10 μM, (a–c) 0, 1, 2, 4 days) and **C2** (10 μM, (d–f) 0, 1, 2, and 3 days) at different pH values over time in a buffered solution with phosphate (100 μM) and 1% DMSO. Absorbance spectra of building block components (pH 7.1 buffered solution with phosphate (100 μM) with 5% DMSO): (g) linker **1** (25 μM). (h) Pd(II) complex **2**·NO_3 (50 μM). (i) Cavitand **3** (25 μM). (j) Ligand **S2** (20 μM).

affinity is likely attributed to the weaking of the hydrophobic effect and competition of DMSO molecules with DOXO for the cavity of the cage.

^{1}H NMR titration experiments have also been undertaken to further corroborate the formation of the host–guest [DOXO⊂cage] complexes. At the cage concentration needed for NMR experiments (≈0.5–1 mM), it was found that both **C1** and **C2** are not soluble enough in D_2O to make a meaningful comparison to the fluorescence titrations. Also considering that the use of organic solvents is much less relevant to binding under biological conditions, no attempt was made to quantify encapsulation by NMR. Nonetheless, the changes in individual chemical shifts provide localised information that is not provided from emission data. From these experiments we observed small chemical shift changes consistent with binding (see ESI Section 4 and Fig. S24–S26†). Remarkably, it was observed an upfield shift of the inward-facing protons of the cages evidencing the encapsulation of DOXO inside the cavity of both **C1** and **C2** cages. Similar observations of small chemical shift changes and large fluorescence changes upon anticancer drug encapsulation have been described in similar works.[51]

Cage disassembly experiments in mixed aqueous solution

Disassembly experiments of cages **C1** and **C2** were performed at different pH values (pH 5.6, 7.2, and 7.8) in DMSO/phosphate buffer. This process was initially studied by UV-visible spectroscopy by monitoring the decrease in the absorption band centred at 300–320 nm characteristic of each cage, and not present in the building block components (see ESI†) as a function of time (Fig. 6). The UV-visible spectra of molecular cage **C1**·NO_3 shows a decrease in absorbance over several days at all of the three different pH values 5.6, 7.2, and 7.8 (Fig. 5a–c). In contrast, the UV-visible spectra of molecular cage **C2** remained unchanged over time (0–3 days) under neutral and basic conditions (Fig. 5e and f) but showed a decrease in absorbance at pH 5.6 (Fig. 5d). These results would suggest that **C1**·NO_3 and **C2** disassemble *via* different mechanisms; the metallo-organic cage is likely degraded by coordination of the phosphate buffer anion to the palladium (see ^{1}H NMR experiments below), resulting in ligand displacement, while the pure organic cage dissociates through acid-catalysed hydrolysis of the hydrazone bonds. The time scale of the hydrolysis is relevant in a biological context as the sustained delivery of drugs over several days is a desirable property in anticancer drug delivery.[70]

Further evidence for a ligand displacement process was obtained by recording the ^{1}H NMR spectra of **C1**·NO_3 in DMSO-d_6 before and after the addition of phosphate buffer after *ca.* 5 min (Fig. 6). Addition of buffer results in upfield shifting of the pyridyl moiety protons (H_f, H_i, H_j, H_k), which is in agreement with the loss of the inductive effect associated with coordination to Pd(II). Furthermore, a comparison to the ^{1}H NMR spectra of free ligand clearly indicates that this species is released intact without hydrolysis of the hydrazone bond. The fast disassembly observed in the NMR experiments (in *ca.* 5 min) is associated to the larger concentration of buffer with respect to cage, as we observed a slower kinetics reducing the buffer concentration (see ESI†). Unfortunately, the low solubility of cage **C2** at the required concentrations for NMR, as well as the broad features

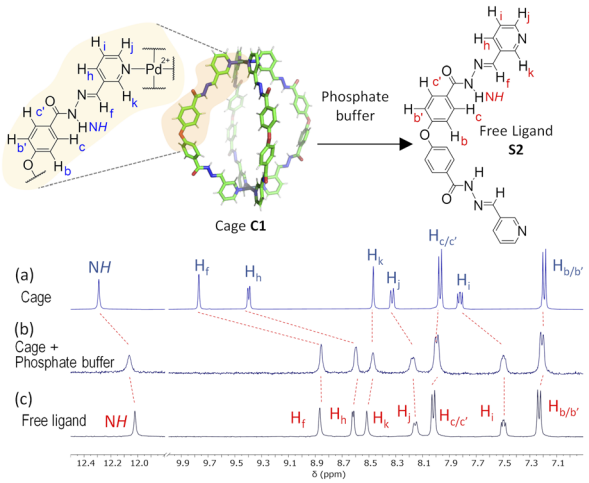

Fig. 6 ^{1}H NMR disassembly experiment of **C1·NO$_3$** in DMSO-d_6 (0.5 mM, 550 μL) with phosphate buffer (pH 7.2, 100 mM, 50 μL). (a) ^{1}H NMR spectra of cage **C1·NO$_3$**. (b) ^{1}H NMR spectrum after the addition of phosphate buffer (*ca.* 5 min), causing cage disassembly. (c) ^{1}H NMR spectra of free ligand (see structure **S2** in ESI†).

of these spectra in phosphate buffer/DMSO have hindered a similar study.

Overall, these stability experiments highlight some of the challenges in using metallo-organic cages for bio-medical applications.[6] They also show that pure organic cages may be better suited to this purpose. Moreover, the selective hydrolysis of the hydrazone bonds in **C2** at slightly acidic pH presents an ideal scenario for stimuli responsive drug delivery at the acidic microenvironment of a tumor.

Biological studies

Toxicity studies were first performed to determine the biocompatibility of the empty cages. Tumoral 4T1 (murine triple-negative breast cancer) and human melanoma SK-Mel-103 cell lines were treated with increasing concentrations of **C1·NO$_3$** and **C2** and cell viability was measured at 48 h (Fig. 7). The **C1·NO$_3$** palladium cage produced toxicity at low concentrations (viability lower than 80% was found at concentration of the cage of 3.12 μM in agreement with previous works on metallo-organic cages),[40,71] whereas the organic cage **C2** was shown to be non-toxic at concentrations as high as 25–50 μM. We also examined that the building blocks components of cage **C2** (ligand **1** and calixarene **3**) are non-toxic (Fig. S37a in ESI†). Selecting the less toxic organic cage **C2** for encapsulation studies, when cancer cells were treated with the [DOXO⊂**C2**] cage, an antitumoral effect was achieved in 4T1 and SK-Mel-103 cells attributed to cage internalisation and cage disassembly in the lysosomes. This is supported by comparing cells treated with the building blocks components of cage **C2** (Ligand **1** and calixarene **3**) and DOXO (**1** + **3** + DOXO) with cells treated with [DOXO⊂**C2**]. In both cases, [DOXO⊂**C2**], and **1** + **3** + DOXO, a comparable antitumoral effect is achieved indicating that the efficacy of DOXO remains unaffected by the **C2** framework or [DOXO⊂**C2**] formation (Fig. 7c, d and S37b in ESI†).

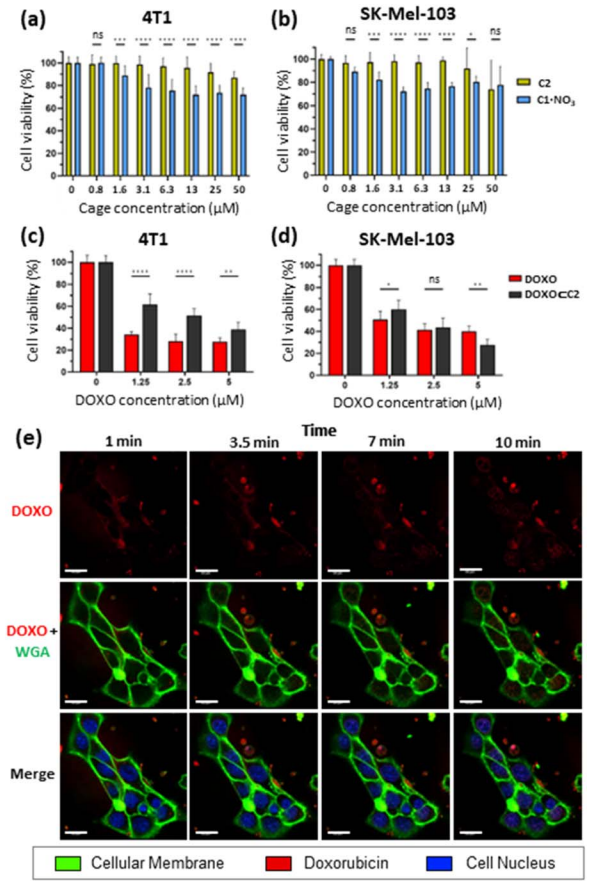

Fig. 7 Cell viability measured by WST-1. Data represented as mean ± SEM ($n = 3$). Toxicity assay with organic cage **C2** (yellow) and palladium metallo-organic cage **C1·NO$_3$** (blue) on: (a) 4T1 cells and (b) SK-Mel-103 cells. Treatment with DOXO⊂**C2** complex (black) and free doxorubicin (red) on: (c) 4T1 cells and (d) SK-Mel-103 cells. Increasing concentrations of DOXO and a fixed concentration of organic cage **C2** (25 μM) was used to obtain 95% encapsulation of DOXO. (e) Time-lapse confocal images of SK-Mel-103 cells incubated with Hoechst (blue nuclei marker), WGA (green membrane marker) and treated with the DOXO⊂**C2** complex (fluorescent red) at 5 μM up to 10 min. Scale bar represents 20 μm.

Additionally, the treatment with free DOXO resulted in a slightly enhanced antitumoral effect. This can be attributed to the efficient entrapment of the free drug, leading to differential internalisation and processing of [DOXO⊂**C2**] by cancer cells (*vide infra* and Fig. 7c and d). Nevertheless, the results indicate that the activity of DOXO is fully recovered upon its release from [DOXO⊂**C2**]. Overall, these results highlights the suitability of the organic cage for drug delivery and the low toxicity of the unloaded organic cage compared to the metallo-organic cage.

To assess the internalisation of the molecular cages, cellular uptake studies of the doxorubicin-encapsulated organic cage were focused on SK-Mel-103 cells. Time-lapse confocal images revealed an increase in DOXO fluorescence (in red) within the cytoplasm of cells (limited by membrane marker in green) that finally reaches the nuclei (in blue) of the cells (Fig. 7). The rapid internalisation, within minutes, suggests passive diffusion as a mechanism of cellular uptake. Although, membrane

permeability is typically limited to molecules with sizes of 1500 Å^3,[72–75] (cage **C2** has a molecular volume of 2600 Å^3 just slightly over the limit) several works have demonstrated that cages of various sizes can cross cell membranes and deliver anticancer drugs in cells.[37,41,42,45,48,53,76,77] Analogous time-dependent confocal images with free DOXO confirmed the different drug-internalisation ratio when compared with [DOXO⊂**C2**] (Fig. S38 in ESI†). The images showed a faster diffusion of DOXO from cellular medium to the cells, with a large amount accumulated in the nucleus after 10 minutes compared to [DOXO⊂**C2**]. Overall, our studies indicate the proper formation of [DOXO⊂**C2**] cage and ability to enter in cells and deliver DOXO.

Conclusions

In this work we have compared a similarly shaped metallo-organic cage and a fully organic cage. We found that the organic cage **C2** is a promising drug delivery system, with clear advantages over the analogue the palladium cage **C1**. Both cages are water-soluble requiring only a 1–5% of DMSO to achieve micromolar concentrations, which is compatible with *in vitro* cell culture experiments. The organic cage **C2** remains intact in neutral pH phosphate buffer, unlike the palladium cage **C1**, which breaks down under similar conditions. Cage **C2** has a high binding affinity towards the anticancer drug doxorubicin (DOXO), allowing efficient encapsulation at the micromolar concentration required for biological drug delivery. In contrast, **C1**·$\mathbf{NO_3}$ exhibits weaker binding and disassembly by interaction with DOXO, lacking sufficient binding affinity and stability. In addition, cage disassembly takes place when cage **C2** is placed in a slightly acidic pH, making the cage an ideal pH-responsive drug delivery system. In addition to the excellent chemical properties, cage **C2** exhibits a remarkable cellular compatibility. Cage **C2** does not shows any cellular toxicity even at high doses (25–50 μM), in contrast to the significant toxicity observed in **C1**. Additionally, cage **C2** effectively delivers DOXO to cells from the DOXO⊂**C2** complex, preserving the cytotoxic activity of this anticancer drug. Overall, the organic cage **C2** is a proof-of-concept low toxicity drug delivery system that shows an excellent performance in cells. These results highlight the possibility of using pure organic molecular cages as suitable drug-delivery systems due to their absence of toxicity compared to metalloorganic cages.

Data availability

Data associated to the manuscript is available as ESI† in PDF format and the crystal structure data in CIF format.

Author contributions

The manuscript was written through contributions of all authors. All authors have given approval to the final version of the manuscript.

Conflicts of interest

There are no conflicts to declare.

Acknowledgements

V. M.-C. acknowledges the financial support from project CIDEGENT/2020/031 funded by the Generalitat Valenciana, project PID2020-113256RA-I00 funded by MICIU/AEI/10.13039/501100011033, and project CNS2023-144879 funded by MICIU/AEI/10.13039/501100011033 and European Union NextGenerationEU/PRTR. R. M.-M. acknowledges the financial support from project PROMETEO CIPROM/2021/007 from the Generalitat Valenciana and project PID2021-126304OB-C41 funded by MICIU/AEI/10.13039/501100011033 and FEDER A way to make Europe. G. M.-G. acknowledges the financial support from the mobility grant CIBEFP/2022/43 funded by the Generalitat Valenciana. D. B.-R. acknowledges the financial support from fellowship CIACIF/2022/174 funded by the Generalitat Valenciana. The authors thank "Servei Central d'Instrumentació Científica (SCIC)" at Universitat Jaume I, and mass spectrometry, proteomics laboratory member of Proteored, and single crystal X-ray diffraction facilities of SCSIE at Universitat de València. NMR spectra were registered at the U26 facility of ICTS "NANBIOSIS". This research was supported by CIBER-Consorcio Centro de Investigación Biomédica en Red (CB06/01/2012), Instituto de Salud Carlos III, Ministerio de Ciencia e Innovación.

References

1 J. W. Steed and J. L. Atwood, *Supramolecular Chemistry*, John Wiley & Sons, Chichester, UK, 3rd edn, 2022.
2 J.-M. Lehn, *Supramolecular Chemistry: Concepts and Perspectives*, VCH, Weinheim, Germany, 1995.
3 F. Diederich, *Angew. Chem., Int. Ed.*, 2007, **46**, 68–69, DOI: **10.1002/anie.200602704**.
4 J.-M. Lehn, *Eur. Rev.*, 2009, **17**, 263–280, DOI: **10.1017/s1062798709000805**.
5 G. Montà-González, F. Sancenón, R. Martínez-Máñez and V. Martí-Centelles, *Chem. Rev.*, 2022, **122**, 13636–13708, DOI: **10.1021/acs.chemrev.2c00198**.
6 E. G. Percástegui, T. K. Ronson and J. R. Nitschke, *Chem. Rev.*, 2020, **120**, 13480–13544, DOI: **10.1021/acs.chemrev.0c00672**.
7 R. Chakrabarty, P. S. Mukherjee and P. J. Stang, *Chem. Rev.*, 2011, **111**, 6810–6918, DOI: **10.1021/cr200077m**.
8 Y. Jin, Q. Wang, P. Taynton and W. Zhang, *Acc. Chem. Res.*, 2014, **47**, 1575–1586, DOI: **10.1021/ar500037v**.
9 X. Yang, Z. Ullah, J. F. Stoddart and C. T. Yavuz, *Chem. Rev.*, 2023, **123**, 4602–4634, DOI: **10.1021/acs.chemrev.2c00667**.
10 V. Martí-Centelles, *Tetrahedron Lett.*, 2022, **93**, 153676, DOI: **10.1016/j.tetlet.2022.153676**.
11 O. Vestrheim, M. E. Schenkelberg, Q. Dai and S. T. Schneebeli, *Org. Chem. Front.*, 2023, **10**, 3965–3974, DOI: **10.1039/d3qo00480e**.

12 X. Liu, A. Wang, C. Wang, J. Li, Z. Zhang, A. M. Al-Enizi, A. Nafady, F. Shui, Z. You, B. Li, Y. Wen and S. Ma, *Nat. Commun.*, 2023, **14**, 7022, DOI: **10.1038/s41467-023-42833-y**.
13 D. Zhang, T. K. Ronson, Y.-Q. Zou and J. R. Nietschke, *Nat. Rev. Chem*, 2021, **5**, 168–182, DOI: **10.1038/s41570-020-00246-1**.
14 A. Pöthig and A. Casini, *Theranostics*, 2019, **9**, 3150–3169, DOI: **10.7150/thno.31828**.
15 T. K. Piskorz, V. Martí-Centelles, R. L. Spicer, F. Duarte and P. J. Lusby, *Chem. Sci.*, 2023, **14**, 11300–11331, DOI: **10.1039/D3SC02586A**.
16 V. Martí-Centelles, A. L. Lawrence and P. J. Lusby, *J. Am. Chem. Soc.*, 2018, **140**, 2862–2868, DOI: **10.1021/jacs.7b12146**.
17 Y. Yu, J. M. Yang and J. Rebek, *Chem*, 2020, **6**, 1265–1274, DOI: **10.1016/j.chempr.2020.04.014**.
18 A. Pappalardo, R. Puglisi and G. Trusso Sfrazzetto, *Catalysts*, 2019, **9**, 630, DOI: **10.3390/catal9070630**.
19 S. Chen and L.-J. Chen, *Chemistry*, 2022, **4**, 494–519, DOI: **10.3390/chemistry4020036**.
20 A. Galan and P. Ballester, *Chem. Soc. Rev.*, 2016, **45**, 1720–1737, DOI: **10.1039/c5cs00861a**.
21 P. Mal, B. Breiner, K. Rissanen and J. R. Nitschke, *Science*, 2009, **324**, 1697–1699, DOI: **10.1126/science.1175313**.
22 T. Y. Kim, R. A. S. Vasdev, D. Preston and J. D. Crowley, *Chem.–Eur. J.*, 2018, **24**, 14878–14890, DOI: **10.1002/chem.201802081**.
23 S. La Cognata and V. Amendola, *Chem. Commun.*, 2023, **59**, 13668–13678, DOI: **10.1039/D3CC04522F**.
24 M. A. Little and A. I. Cooper, *Adv. Funct. Mater.*, 2020, **30**, 1909842, DOI: **10.1002/adfm.201909842**.
25 J. Zhang, S. Xie, M. Zi and L. Yuan, *J. Sep. Sci.*, 2020, **43**, 134–149, DOI: **10.1002/jssc.201900762**.
26 G. Zhang and M. Mastalerz, *Chem. Soc. Rev.*, 2014, **43**, 1934–1947, DOI: **10.1039/c3cs60358j**.
27 W. Liu and J. F. Stoddart, *Chem*, 2021, **7**, 919–947, DOI: **10.1016/j.chempr.2021.02.016**.
28 N. Judge, L. Wang, Y. Y. L. Ho and Y. Wang, *Macromol. Res.*, 2018, **26**, 1074–1084, DOI: **10.1007/s13233-018-6156-3**.
29 A. Casini, B. Woods and M. Wenzel, *Inorg. Chem.*, 2017, **56**, 14715–14729, DOI: **10.1021/acs.inorgchem.7b02599**.
30 W. Dou, C.-Y. Yang, L.-R. Hu, B. Song, T. Jin, P.-P. Jia, X. Ji, F. Zheng, H.-B. Yang and L. Xu, *ACS Mater. Lett.*, 2023, **5**, 1061–1082, DOI: **10.1021/acsmaterialslett.2c01147**.
31 N. Ahmad, H. A. Younus, A. H. Chughtai and F. Verpoort, *Chem. Soc. Rev.*, 2015, **44**, 9–25, DOI: **10.1039/c4cs00222a**.
32 D. Sun, X. Feng, X. Zhu, Y. Wang and J. Yang, *Coord. Chem. Rev.*, 2024, **500**, 215546, DOI: **10.1016/j.ccr.2023.215546**.
33 G. Montà-González, E. Ortiz-Gómez, R. López-Lima, G. Fiorini, R. Martínez-Máñez and V. Martí-Centelles, *Molecules*, 2024, **29**, 1621, DOI: **10.3390/molecules29071621**.
34 C. Zhu, M. Pan and C. Su, Metal-Organic Cages for Biomedical Applications, *Isr. J. Chem.*, 2019, **59**, 209–219, DOI: **10.1002/ijch.201800147**.
35 L. Tapia, I. Alfonso and J. Solà, *Org. Biomol. Chem.*, 2021, **19**, 9527–9540, DOI: **10.1039/D1OB01737C**.
36 J. Zhou, G. Yu and F. Huang, *Chem. Soc. Rev.*, 2017, **46**, 7021–7053, DOI: **10.1039/c6cs00898d**.
37 I. A. Bhat, R. Jain, M. M. Siddiqui, D. K. Saini and P. S. Mukherjee, *Inorg. Chem.*, 2017, **56**, 5352–5360, DOI: **10.1021/acs.inorgchem.7b00449**.
38 S. Senapati, A. K. Mahanta, S. Kumar and P. Maiti, *Signal Transduction Targeted Ther.*, 2018, **3**, 7, DOI: **10.1038/s41392-017-0004-3**.
39 M. J. Webber and R. Langer, *Chem. Soc. Rev.*, 2017, **46**, 6600–6620, DOI: **10.1039/c7cs00391a**.
40 A. Schmidt, V. Molano, M. Hollering, A. Pöthig, A. Casini and F. E. Kühn, *Chem.–Eur. J.*, 2016, **22**, 2253–2256, DOI: **10.1002/chem.201504930**.
41 Y.-R. Zheng, K. Suntharalingam, T. C. Johnstone and S. Lippard, *Chem. Sci.*, 2015, **6**, 1189–1193, DOI: **10.1039/c4sc01892c**.
42 Z. Yue, H. Wang, D. J. Bowers, M. Gao, M. Stilgenbauer, F. Nielsen, J. T. Shelley and Y.-R. Zheng, *Dalton Trans.*, 2018, **47**, 670–674, DOI: **10.1039/c7dt03537c**.
43 J. E. M. Lewis, E. L. Gavey, S. A. Cameron and J. D. Crowley, *Chem. Sci.*, 2012, **3**, 778–784, DOI: **10.1039/C2SC00899H**.
44 L. S. Lisboa, M. Riisom, H. J. Dunne, D. Preston, S. M. F. Jamieson, L. J. Wright, C. G. Hartinger and J. D. Crowley, *Dalton Trans.*, 2022, **51**, 18438–18445, DOI: **10.1039/D2DT02720H**.
45 Y. Fang, X. Lian, Y. Huang, G. Fu, Z. Xiao, Q. Wang, B. Nan, J.-P. Pellois and H.-C. Zhou, *Small*, 2018, **14**, 1802709, DOI: **10.1002/smll.201802709**.
46 H. Wang, Z. Qiu, H. Liu, A. M. D. S. Jayawardhana, Z. Yue, H. Daghlas, D. J. Bowers, B. Datta and Y.-R. Zheng, *Front. Chem.*, 2019, **7**, 39, DOI: **10.3389/fchem.2019.00039**.
47 B. Therrien, G. Süss-Fink, P. Govindaswamy, A. K. Renfrew and P. J. Dyson, *Angew. Chem., Int. Ed.*, 2008, **47**, 3773–3776, DOI: **10.1002/anie.200800186**.
48 A. Ahmedova, R. Mihaylova, D. Momekova, P. Shestakova, S. Stoykova, J. Zaharieva, M. Yamashina, G. Momekov, M. Akita and M. Yoshizawa, *Dalton Trans.*, 2016, **45**, 13214–13221, DOI: **10.1039/c6dt01801g**.
49 F. Schmitt, J. Freudenreich, N. P. E. Barry, L. Juillerat-Jeanneret, G. Süss-Fink and B. Therrien, *J. Am. Chem. Soc.*, 2012, **134**, 754–757, DOI: **10.1021/ja207784t**.
50 W.-Y. Li, C.-W. Zhao, Y.-F. Zhang, Q. Guan, J.-J. Wan, J.-P. Ma, Y.-A. Li and Y.-B. Dong, *Chem. Commun.*, 2021, **57**, 7954–7957, DOI: **10.1039/D1CC02629A**.
51 V. W. Liyana Gunawardana, C. Ward, H. Wang, J. H. Holbrook, E. R. Sekera, H. Cui, A. B. Hummon and J. D. Badjić, *Angew. Chem., Int. Ed.*, 2023, **62**(33), e202306722, DOI: **10.1002/anie.202306722**.
52 S. M. McNeill, D. Preston, J. E. M. Lewis, A. Robert, K. Knerr-Rupp, D. O. Graham, J. R. Wright, G. I. Giles and J. D. Crowley, *Dalton Trans.*, 2015, **44**, 11129–11136, DOI: **10.1039/c5dt01259g**.
53 A. Ahmedova, D. Momekova, M. Yamashina, P. Shestakova, G. Momekov, M. Akita and M. Yoshizawa, *Chem.–Asian J.*, 2016, **11**, 474–477, DOI: **10.1002/asia.201501238**.
54 J. Kalia and R. T. Raines, *Angew. Chem., Int. Ed.*, 2008, **47**, 7523–7526, DOI: **10.1002/anie.200802651**.

55 F. Seidi, Y. Zhong, H. Xiao, Y. Jin and D. Crespy, *Chem. Soc. Rev.*, 2022, **51**, 6652–6703, DOI: **10.1039/d2cs00099g**.
56 J. Xu, B. Qin, S. Luan, P. Qi, Y. Wang, K. Wang and S. Song, *J. Bioact. Compat. Polym.*, 2018, **33**, 119–133, DOI: **10.1177/0883911517715658**.
57 Y. Bae, S. Fukushima, A. Harada and K. Kataoka, *Angew. Chem., Int. Ed.*, 2003, **42**, 4640–4643, DOI: **10.1002/anie.200250653**.
58 D. K. Kölmel and E. T. Kool, *Chem. Rev.*, 2017, **117**, 10358–10376, DOI: **10.1021/acs.chemrev.7b00090**.
59 P. T. Corbett, J. Leclaire, L. Vial, K. R. West, J.-L. Wietor, J. K. M. Sanders and S. Otto, *Chem. Rev.*, 2006, **106**, 3652–3711, DOI: **10.1021/cr020452p**.
60 E. Boedtkjer and S. F. Pedersen, *Annu. Rev. Physiol.*, 2020, **82**, 103–126, DOI: **10.1146/annurev-physiol-021119-034627**.
61 Z. Fülöp, R. Gref and T. Loftsson, *Int. J. Pharm.*, 2013, **454**, 559–561, DOI: **10.1016/j.ijpharm.2013.06.058**.
62 Y. Lin, J. Sun, M. Tang, G. Zhang, L. Yu, X. Zhao, R. Ai, H. Yu, B. Shao and Y. He, *Anal. Chem.*, 2021, **93**, 6544–6550, DOI: **10.1021/acs.analchem.1c00723**.
63 M. A. Zwijnenburg, E. Berardo, W. J. Peveler and K. E. Jelfs, *J. Phys. Chem. B*, 2016, **120**, 5063–5072, DOI: **10.1021/acs.jpcb.6b03059**.
64 K. A. Connors, *Binding Constants: The Measurement of Molecular Complex Stability*, John Wiley & Sons, New York, 1987.
65 R Core Team, *2015, R: A Language and Environment for Statistical Computing*, R Foundation for Statistical Computing, Vienna, Austria, **https://www.R-project.org/**, accessed 10th October 2023.
66 Studio Team, *2015, RStudio: Integrated Development for R, version 0.99.892*, RStudio, Inc., Boston, MA, **https://www.rstudio.com/**, accessed 10th October 2023.
67 D. P. August, G. S. Nichol and P. J. Lusby, *Angew. Chem., Int. Ed.*, 2016, **55**, 15022–15026, DOI: **10.1002/anie.201608229**.
68 V. Martí-Centelles, T. K. Piskorz and F. Duarte, *ChemRxiv*, 2024, preprint, DOI: **10.26434/chemrxiv-2024-fmlx0**.
69 C. H. Haas, S. M. Biros and J. Rebek, *Chem. Commun.*, 2005, **48**, 6044–6045, DOI: **10.1039/b513408k**.
70 C. Pacheco, A. Baião, T. Ding, W. Cui and B. Sarmento, *Adv. Drug Delivery Rev.*, 2023, **194**, 114724, DOI: **10.1016/j.addr.2023.114724**.
71 Z. Xiao, H. Lin, H. F. Drake, J. Diaz, H.-C. Zhou and J.-P. Pellois, *J. Am. Chem. Soc.*, 2023, **145**, 27690–27701, DOI: **10.1021/JACS.3C09918**.
72 P. Matsson and J. Kihlberg, *J. Med. Chem.*, 2017, **60**, 1662–1664, DOI: **10.1021/acs.jmedchem.7b00237**.
73 P. Matsson and B. C. Doak, *Adv. Drug Delivery Rev.*, 2016, **101**, 42–61, DOI: **10.1016/j.addr.2016.03.013**.
74 J. Mosquera, M. Henriksen-Lacey, I. García, M. Martínez-Calvo, J. Rodríguez, J. L. Mascareñas and L. M. Liz-Marzán, *J. Am. Chem. Soc.*, 2018, **140**, 4469–4472, DOI: **10.1021/jacs.7b12505**.
75 J. Rodríguez, J. Mosquera, J. R. Couceiro, J. R. Nitschke, M. E. Vázquez and J. L. Mascareñas, *J. Am. Chem. Soc.*, 2017, **139**, 55–58, DOI: **10.1021/jacs.6b11103**.
76 D. Al Kalabi, A. Dey, L. O. Alimi, H. Puwoński, S. Habuchi and N. M. Khashab, *Chem. Sci.*, 2022, **13**, 7341–7346, DOI: **10.1039/D2SC00836J**.
77 Y. Liang, Y. Fang, Y. Cui and H. Zhou, *Nano Res.*, 2021, **14**, 3407–3415, DOI: **10.1007/s12274-021-3646-y**.